

# FE modelling of microstructure evolution during friction stir spot welding in AA6082-T6

Z. Gao · J. T. Niu · F. Krumphals · N. Enzinger ·  
S. Mitsche · C. Sommitsch

Received: 24 September 2012 / Accepted: 8 July 2013 / Published online: 19 July 2013  
© International Institute of Welding 2013

**Abstract** Friction stir spot welding (FSSW) is a solid-state joining method, which is a variant of friction-stir welding. Microstructure analysis shows that the FSSW joint contains four different zones, namely the stir zone, thermo-mechanical affected zone, heat-affected zone and base metal, respectively. In this paper, the results of a FE analysis of the FSSW process of AA6082-T6 considering geometric dynamic recrystallization are presented. A physically based model taking into account three internal state variables was implemented into the commercial FE package DEFORM-3D to describe the microstructure evolution during FSSW. This model allows predicting the dislocation density, grain size, temperature, effective strain, and strain rate during FSSW. The microstructure

in stir zone was analysed by electron backscattered diffraction. Experimental and simulation results have been compared to validate the model.

**Keywords** Microstructure evolution · FEM · Friction stir spot welding · AA6082-T6 · Finite element analysis · Microstructure

## 1 Introduction

The friction stir welding process was developed by TWI, Abington, UK in 1991 for joining light alloys such as aluminium. Friction stir spot welding (FSSW) is a variant of friction stir welding and it is primarily used in automotive industry as a partial replacement of resistance spot welding.

The stages of FSSW process and the formed weld zones are schematically shown in Fig. 1:

- The process starts with rotating the tool with high-rotational speed and plunging into a work piece.
- After the shoulder contacts the top surface of the work piece, joining takes place due to the pressure and temperature causing inter-diffusion of the involved materials across the interface at atomic level.
- Finally, when a predetermined penetration is reached, the process dwells for a little while. Afterwards, the tool retracts from the work piece.

The material in the stir zone is changed significantly due to high temperatures and stresses acting during the process. The FSSW joint contains four different zones, namely the stir zone, thermo-mechanical affected zone (TMAZ), heat-affected zone and the unaffected base metal, respectively [1,2].

In materials with high-stacking fault energy such as aluminium and its alloys, dynamic recovery and static recrystallization are the main restoration processes during and after

---

Doc. IIW-2401, recommended for publication by Commission IX  
"Behaviour of Metals Subjected to Welding."

Z. Gao (✉) · J. T. Niu  
School of Materials Science and Engineering, Henan Polytechnic  
University, Jiaozuo, Henan 454000, China  
e-mail: mrgaozeng@163.com

J. T. Niu  
e-mail: niujitai@163.com

Z. Gao · F. Krumphals · N. Enzinger · C. Sommitsch  
Institute for Materials Science and Welding, Graz University of  
Technology, Graz, Austria

F. Krumphals  
e-mail: friedrich.krumphals@tugraz.at

N. Enzinger  
e-mail: norbert.enzinger@tugraz.at

C. Sommitsch  
e-mail: christof.sommitsch@tugraz.at

Z. Gao · F. Krumphals · N. Enzinger · C. Sommitsch  
JOIN 4 + – Network of Excellence for Joining, Graz, Austria

S. Mitsche  
Institute for Electron Microscopy and Fine Structure Research  
(FELMI), Graz University of Technology, Graz, Austria  
e-mail: stefan.mitsche@felmi-zfe.at

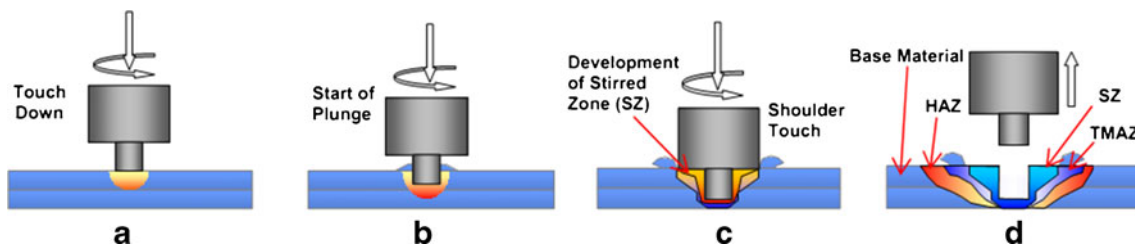


**Fig. 1** Schematic of general FSSW process; **a** touchdown of the pin, **b** start of pin penetration to commence plunge, **c** plunge ends by the shoulder touch and development of weld zones **d** with/without dwell time retraction of the tool with weld zones formed

thermo-mechanical treatment. At specific boundary conditions, such as chemical composition, initial grain size, accumulated strain, strain rate and temperature, geometric dynamic recrystallization (GDRX) can occur during hot deformation of aluminium alloy [3]. GDRX is a process in which a fine and nearly equiaxed grain structure is formed. In GDRX, the original grains flatten at large strain. Meanwhile, the grain boundaries become serrated as subgrain form. Eventually, at a critical strain, the original grain size is reduced to one to two subgrain diameters, at which time the original grain boundaries begin contacting each other at the serrations, causing grain portions to pinch-off [4,5]. GDRX is originated in the 1980s with work on elevated-temperature deformation aluminium to large strains. In this case, substantial grain refinement occurs. This concept has since been carefully verified in pure Al, as well as Al–Mg alloys deforming in the three-power regime. It appears that GDRX is a general phenomenon that can lead to grain refinement in the absence of any discontinuous dynamic recrystallization or continuous dynamic recrystallization. This may be particularly relevant to severe plastic deformation such as rolling and equal-channel angular pressing where dramatic increases in the number of high-angle boundaries are observed [6,7].

During the FSSW process, due to the high-speed revolution of the pin tool in the work piece, the aluminium AA6082-T6 under the tool can achieve a very high strain, strain rate as well

as temperature. In this case, GDRX is easily to occur instead of dynamic recovery. In this contribution, a physically based model considering GDRX taking into account three internal state variables was implemented into the commercial FE package DEFORM-3D to describe the microstructure evolution during FSSW of AA6082-T6. This model allows predicting the dislocation density, grain size, temperature, effective strain and strain rate during FSSW. Experimental and simulation results have been compared to validate the model.

## 2 Numerical model of friction stir spot welding

The assembly of the numerical model can be seen in Fig. 2. It consists of three parts: tool, workpiece and back plate. The size of workpiece is  $60 \times 60 \times 4$  mm. In order to optimise the resolution close to the tool and minimise the computational expenses, non-uniform mesh density with automatic remeshing was applied in the work piece, whose finer mesh size under the tool was set to 0.75 mm and the other mesh size was set to 1.5 mm. For the auto remeshing during numerical simulation, tetrahedron element was used in DEFORM-3D. During the deformation process, the relative interference depth 0.7 is used for the remesh criteria.

For the work piece of AA6082-T6, a rigid-viscoplastic temperature, strain and strain rate-dependent material model was utilised. Figure 3 shows the material flow stress curve at

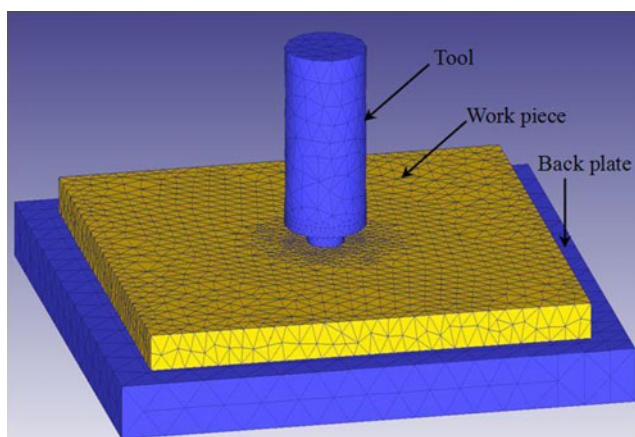


**Fig. 2** Schematic illustration of tool, work piece and back plate

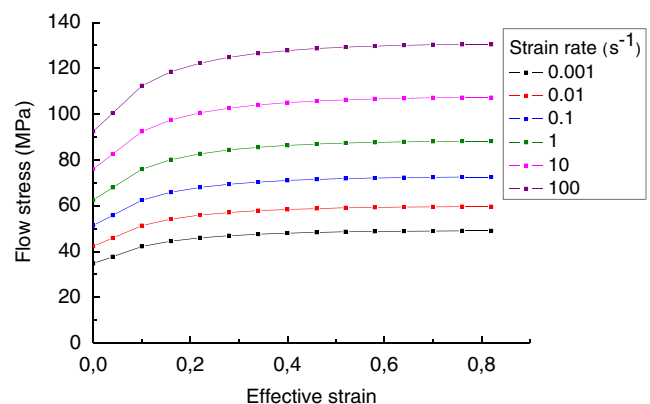


**Fig. 3** Flow stress–strain curves for AA6082-T6 used in the model

**Table 1** Thermal conductivity of AA6082-T6

Temperature (°C)	20	100	200	300	400	500	580
Thermal conductivity (W/m K)	215	212	215	216	208	202	196

300 °C. The true stress–strain data was obtained from isothermal compression tests at temperatures from 300 to 550 °C and strain rates from 0.001 to 100 s<sup>-1</sup>. As far as the thermal characteristics of AA6082-T6 are concerned, the following constant values were utilised: heat capacity 889 [J/kg K], convection coefficient 20 [W/m<sup>2</sup> K] and emissivity 700 [W/m<sup>2</sup> K<sup>4</sup>]. Thermal conductivity was taken into account as a function of temperature as shown in Table 1. The utilised tool and back plate were made of hot-work steel H13 and considered as rigid bodies. The default values for both thermal and mechanical properties in DEFORM were used for H13 in this work.

The friction coefficient between tool and work piece is an input parameter in the FE model and is used in heat generation formulations. The constant shear friction model was selected in this study. The friction force is defined by

$$f = mk \quad (1)$$

where  $f$  denotes the frictional stress,  $k$  the shear yield strength and  $m$  the friction factor.

Besides, the temperature in the workpiece will increase with the plastic deformation. The heat density

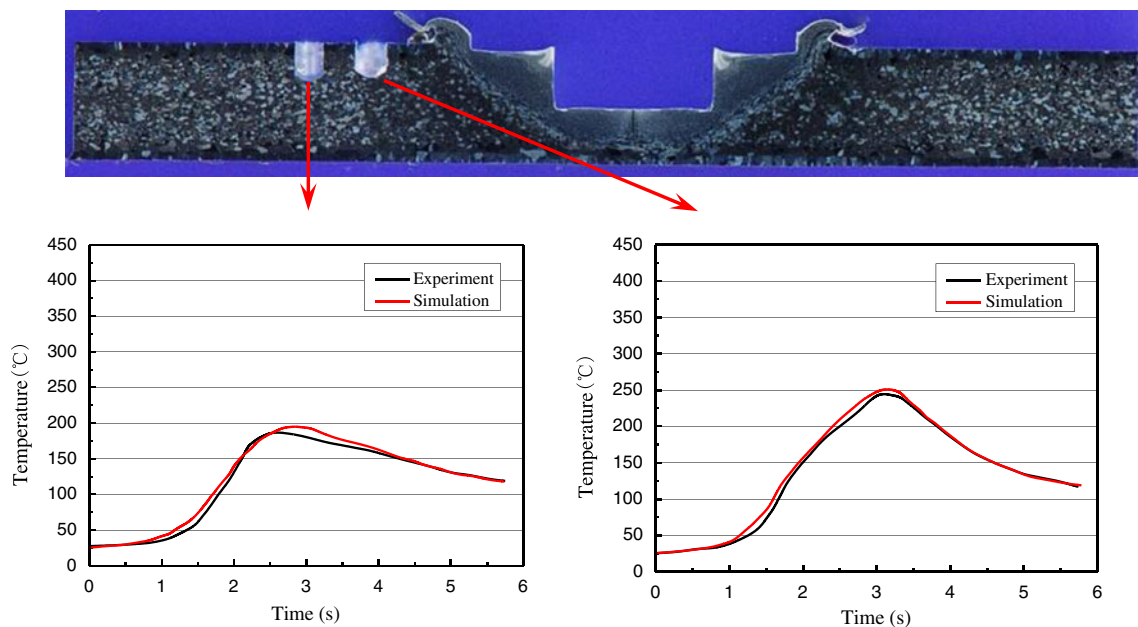
based on plastic deformation can be described as the following:

$$q_p = \alpha_p \bar{\sigma} \dot{\varepsilon} \quad (2)$$

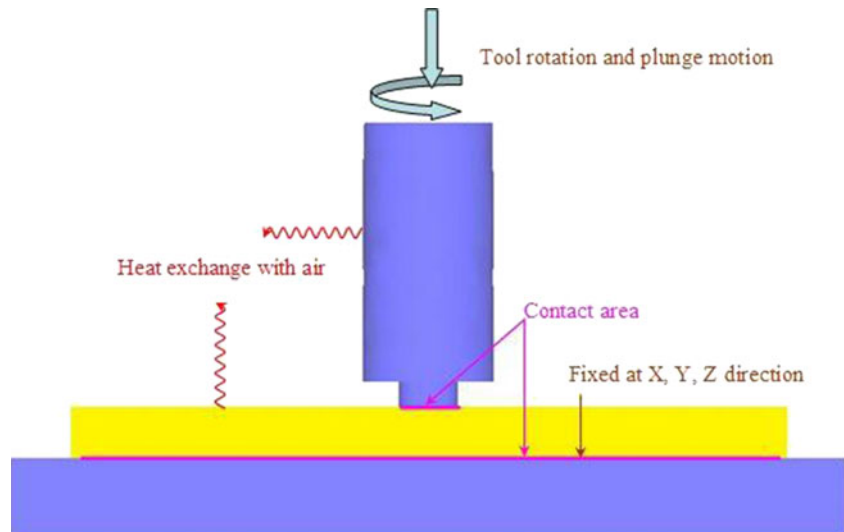
Where  $q_p$  is the heat density due to the plastic deformation,  $\bar{\sigma}$  the equivalent stress,  $\dot{\varepsilon}$  and the effective strain rate.  $\alpha_p$  indicates thermal transition efficiency and the value in this research is 0.95 [8].

To select an appropriate friction factor, it is very important because it has a significant influence on heat generation. If the friction factor is too small, heat generation will be too low to plastify the materials and to weld them, while in the simulation, too large friction factors may result in an unreasonable thermal field. In this research, shear friction factor 0.6 was used. Before the calculation of the microstructure evolution, the experimental and calculated thermal cycles were compared at two points, whose distance to the edge of the shoulder was 3 and 5 mm, respectively. Figure 4 shows that a good match can be achieved between the experimental and calculated thermal cycles.

In this research, the constant ambient temperature 20 °C was utilised. The boundary conditions in friction stir spot

**Fig. 4** Comparison of the experimental and calculated thermal cycles at two points

**Fig. 5** Prescribed boundary conditions in friction stir spot welding model



welding model were shown in Fig. 5. The convection coefficient is 0.02 N/s mm °C. The workpiece was fixed at the bottom with the back plate in X, Y and Z direction instead of clamp.

### 3 Microstructure evolution model

#### 3.1 Dislocation density

During hot deformation, three kinds of dislocations can be distinguished, namely, mobile dislocations ( $\rho_m$ ), immobile dislocations in the cell interior ( $\rho_i$ ) and immobile dislocations in the cell walls ( $\rho_w$ ) as illustrated in Fig. 6.

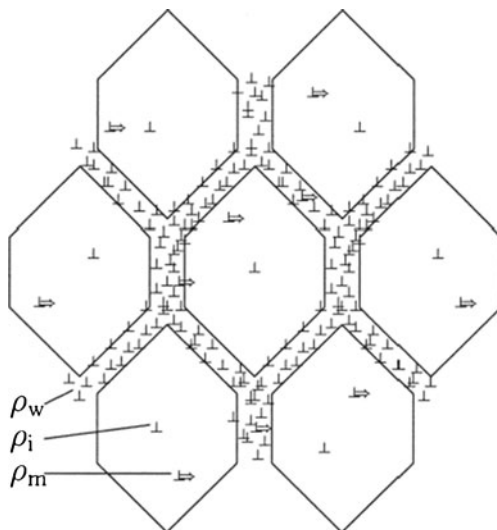


**Fig. 6** Schematic drawing of the arrangement of the three dislocation classes considered in the model: mobile dislocations ( $\rho_m$ ), immobile dislocations in the cell interiors ( $\rho_i$ ) and immobile dislocations in the cell walls ( $\rho_w$ )

During hot deformation, subgrains develop by polygonization with increasing strain. It means that a cellular dislocation arrangement develops, composed of cell walls with high-dislocation density which encloses cell interiors of low-dislocation density.

The density of three kinds of dislocations changes with different mechanisms. Dislocation sources inside the material generate mobile dislocations, interacting with dislocations in the cell interior and dislocations in the cell walls upon their way through the crystal forced by the applied stress to accommodate the imposed strain.

Each mobile dislocation is supposed to glide a mean free path before it is annihilated or immobilised. The density of mobile dislocations can be reduced by the following mechanisms: dislocation annihilations as well as the formation of Lomer–Cottrell dislocations and dipole dislocations [9]. The immobile dislocation density in the cell interior will increase with the formation of Lomer–Cottrell dislocations and decrease with the climbing.

The evolution mechanism of dislocation density in the cell wall is similar with that of immobile dislocations density. Moreover, the dislocation density in the cell wall can be increased by the formation of dipole dislocations.

The kinetics equation of each kind of dislocation can be described as following:

$$\dot{\rho}_x = \rho_x^+ - \rho_x^-, \quad x = m, i, w \quad (3)$$

The initial value for  $\dot{\rho}_x$  ( $x=m, i, w$ ) is  $1.00\text{E}+12 \text{ m/m}^3$ . The total dislocation density in work piece is calculated by the following equation:

$$\rho_{tot} = \rho_m + (1-f_w)\rho_i + f_w\rho_w \quad (4)$$

where  $f_w$  is the volume fraction of the cell walls which is assumed as 0.2 [10].

**Table 2** Process parameters used in experiment and simulation

Rotational speed (l/min)	Plunge depth (mm)	Plunge rate (mm/min)	Dwell time (s)
1,600	2.2	72	3

3.2 Grain structure

In the present paper, the subgrain evolution model developed by Nes combined with GDRX was used. This model is based on the assumption of a cellular microstructure considering the cell size as well as the dislocation density in cell interiors and walls. The subgrain size during high-temperature deformation is given by [9]

$$\delta_{ss} = \left[ K_{\delta} \left( \frac{kT}{Gb^3} \right) \left( \frac{\dot{\epsilon}}{v_D} \right) \exp \frac{U_{SD}}{kT} \right]^{-1/4} \tag{5}$$

where  $\delta_{ss}$  is the subgrain size,  $k$  the Boltzmann constant ( $1.3806504E-23 \text{ JK}^{-1}$ ),  $G$  the shear modulus ( $2.7335E+10 \text{ Pa}$ ),  $b$  the Burgers vector ( $2.86E-10 \text{ m}$ ),  $v_D$  the Debye frequency ( $7.8E+09 \text{ Hz}$ ) and  $U_{SD}$  the activation energy for self diffusion ( $1.8 \text{ eV}$ ) [11],  $T$  the temperature,  $\dot{\epsilon}$  the strain rate and

$$K_{\delta} = [8b^4 \xi_{\delta} q_c^2 C B_{\delta} (1 + f_w (q_b^2 - 1))]^{-1} \tag{6}$$

where

$$q_c = \delta_{ss} \sqrt{\rho_i} \tag{7}$$

and

$$q_b = \sqrt{\frac{\rho_w}{\rho_i}} \tag{8}$$

are the microstructure scaling parameter,  $\xi_{\delta}$  the stress intensity factor (35),  $B_{\delta}$  the pre-exponential constants associated with subgrain growth (511) and  $C$  the proportionality constant (100).

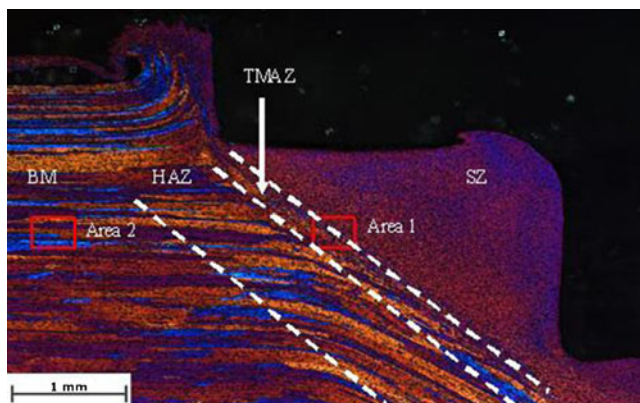


**Fig. 7** Four different zones in a typical FSSW joint

The geometric dynamic recrystallization will take place if a critical strain

$$\epsilon_{cr} = \ln \left( \frac{K_1 D_0 s f}{\delta_{ss}} \right) \tag{9}$$

is exceeded [4], with  $D_0$  specifying the original grain size of the base material AA6082-T6,  $K_1$  a constant of the order of unity, and  $s f$  is the shape factor. In this contribution  $D_0$  is set to  $81.7 \mu\text{m}$ , which is determined by the experimental measurement.

To use an appropriate shape factor ( $s f = \text{grain min/grain max}$ ) is significant for critical strain because all the grains before deformation are more or less elongated, especially for the rolled material. The grain size  $d_{GDRX}$  after GDRX is shown in Eq. (10). It means that the final grain size is proportional to the subgrain size:

$$d_{GDRX} = k_d \delta_{ss} \tag{10}$$

where  $k_d$  is a constant in the range of  $2.5 \pm 1$ .

4 Experimental investigation

The work piece material used in the research is AA6082-T6. Both experiment and numerical simulation were based on the process parameters shown in Table 2. The utilised tool was

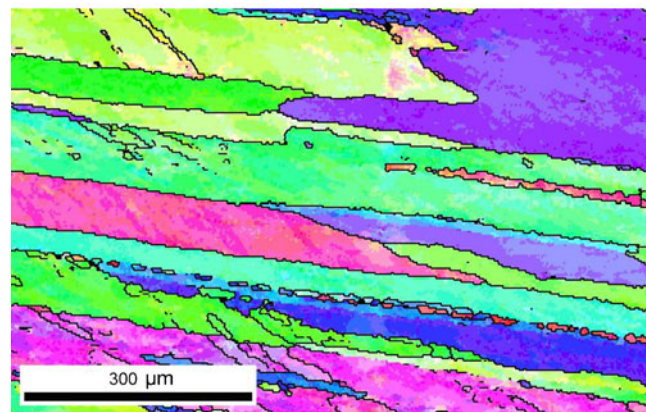
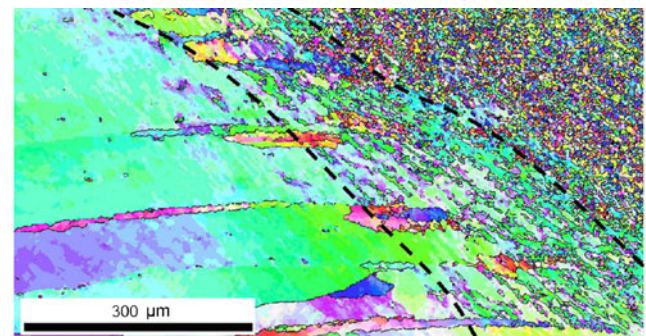
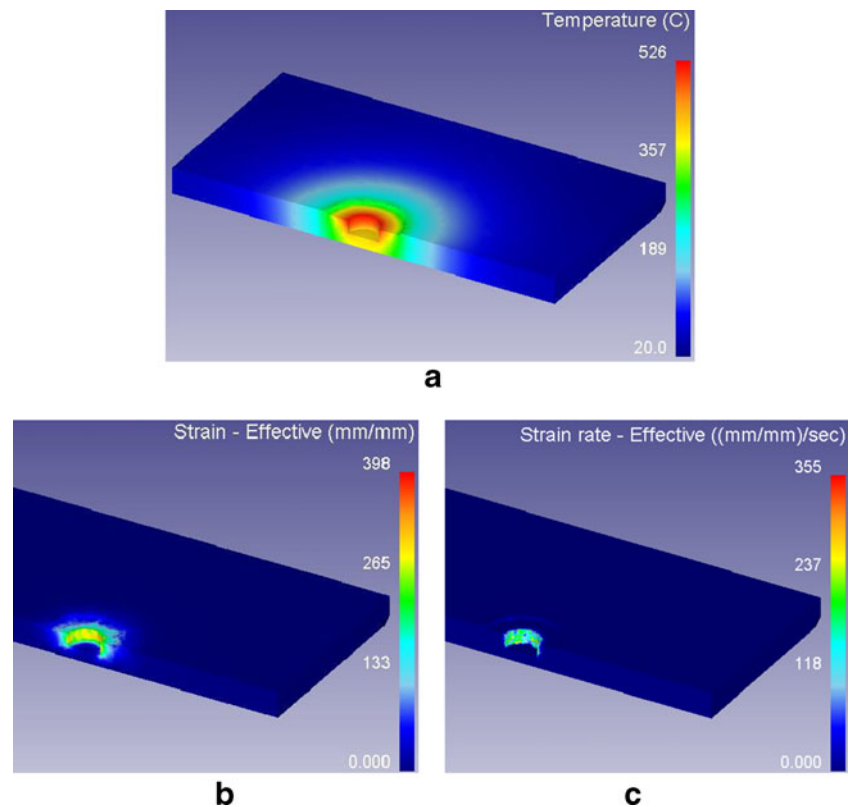


**Fig. 8** Grain structure EBSD image in **a** area 1 and **b** area 2

**Fig. 9** Cut-open view of **a** temperature distribution, **b** effective strain distribution and **c** effective strain rate distribution at the end of FSSW



made of hot-work tool steel H13 and a cylindrical pin was used with the following geometrical characteristics: pin diameter equal to 5.0 mm, pin height 2 mm and shoulder diameter 11 mm. The specimens were quenched by water immediately after FSSW in order to retain the microstructure in the work piece.

It is well accepted that fine and equiaxed grains will be produced after GDRX. For FSSW, process parameters, tool geometry and cooling rate after welding have significant influence on the recrystallized grain size. Figure 7 shows the four different zones in a typical FSSW joint: namely the stir zone, thermo-mechanical affected zone, heat-affected zone and base metal. Two areas were defined to investigate the microstructure.

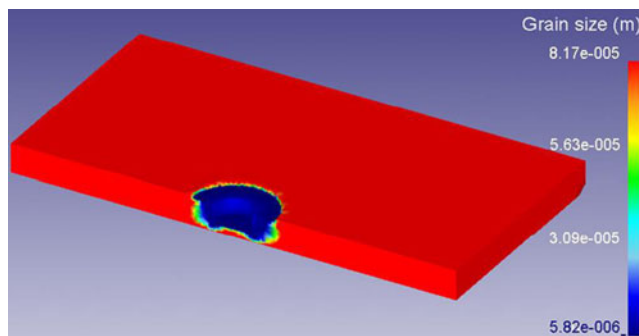


**Fig. 10** FE simulation: distribution of the grain size after FSSW

Figure 8a shows the grain structure electron backscatter diffraction (EBSD) image of TMAZ. TMAZ can be limited by the black dashed lines between the base material and the stir zone. In this region, some material was undergoing GDRX. The stir zone is located at the right side of TMAZ. It is clear that the stir zone is characterised by 100 % fine and equiaxed grains which is one of the principle characteristics of FSSW. The average grain size is around 4.9  $\mu\text{m}$  in the stir zone. Figure 8b shows the microstructure of the base material with an average grain size of 81.7  $\mu\text{m}$ .

## 5 Results and discussion

### 5.1 Calculation of temperature, effective strain and strain rate during FSSW

The basic input data for the microstructure model, temperature, effective strain and strain rate are very important. Figure 9 shows temperature, effective strain and strain rate at the end of process. From the calculation, the peak temperature in the work piece can be estimated to be 526  $^{\circ}\text{C}$ , which is about 0.86 times the solidification temperature (in Kelvin) of the base metal. The temperature distribution is symmetric and maximum temperatures appear at the interface between tool and work piece.

The effective strain at the pin surface and below the shoulder is about 160 mm/mm, which is judged to be very

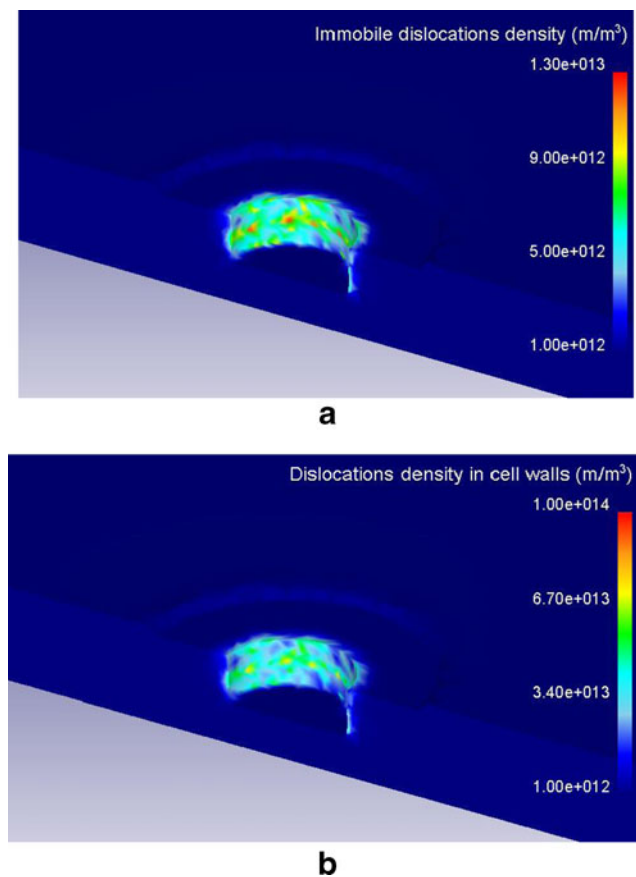


**Fig. 11** Distribution of **a** immobile dislocation density in cell interior and **b** dislocation density in cell walls

high. The effective strain rate at the periphery of the pin is also quite large with values up to 180 (mm/mm)/s. Material just below the shoulder has a relative low strain rate. High strain and strain rate which are characteristic for the FSSW process are significant for GDRX.

## 5.2 Calculation of microstructure evolution during FSSW

The dislocation density model and grain structure model described earlier were implemented into DEFORM-3D to calculate the microstructure evolution during FSSW.

GDRX occurs only if the effective strain exceeds the critical effective strain which is estimated to be 2.0 mm/mm. For FSSW, the effective strain of the material under the tool is extremely high, which can be seen from Fig. 9b. It definitely exceeds the critical effective strain of 2.0 mm/mm. It can be seen in Fig. 10 that the predicted grain size in stir zone at the end of process is around 5.8  $\mu\text{m}$  compared to a measured value of 4.9  $\mu\text{m}$ . In the other area out of the shoulder, the grain size remains unchanged due to the low heat input.

Figure 11 shows the dislocation density in the work piece. The immobile dislocation density in the cell interior is significantly lower than the one in the cell walls. The area with a

relative high-dislocation density is mainly located at the periphery of the pin for both immobile dislocations and cell wall dislocations. The dislocation density in other areas shows no significant change. Compared with cold deformation, the dislocation density in the work piece is lower due to the dislocation climbing and annihilation at high temperatures.

## 6 Conclusions

In this paper, three kinds of dislocations are considered in a physically based model which was implemented into DEFORM-3D. With this model, the microstructure evolution during FSSW process was successfully predicted.

The main achieved results can be summarised as follows:

- (1) After FSSW, the microstructure in the stir zone consists of a fine and equiaxed grain structure. The predicted grain size in the stir zone is around 5.8  $\mu\text{m}$ , which agrees well with the experimental results (4.9  $\mu\text{m}$ ).
- (2) The region of the increased immobile dislocations density and dislocation density in cell walls is mainly located at the periphery of the pin, i.e., in the stir zone. There is only little change of the dislocation density in the base metal.
- (3) During FSSW, the effective strain and strain rate is extremely high due to the high-rotational speed of the tool. The effective strain under the tool is high enough to exceed the critical strain which is necessary for GDRX.

**Acknowledgments** The K-Project Network of Excellence for Joining Technologies JOIN4+ is fostered in the frame of COMET—Competence Centers for Excellent Technologies by BMVIT, BMWFJ, FFG, Land Oberösterreich, Land Steiermark, SFG, and ZIT. The programme COMET is handled by FFG.

## References

1. Khosa S, Weinberger T, Enzinger N (2007) Finite element analysis of material flow patterns in friction stir spot welding of Al 6082-T6 using different process parameters and tool geometries. 5th Int Conf Heat Transf Fluid Mech Thermodyn
2. Mishra RS, Ma ZY (2005) Friction stir welding and processing. Mater Sci Eng, R 50:1–78
3. Poletti C, Rodriguez-Hortalá M, Hauser M, Sommitsch C (2011) Microstructure development in hot deformed AA6082. Mater Sci Eng, A 528:2423–2430
4. Blum W, Zhu Q, Merkel R, McQueen HJ (1996) Geometric dynamic recrystallization in hot torsion of Al-5Mg-0.6Mn. Mater Sci Eng, A 205:23–30
5. Pettersen T, Holmedal B, Nes E (2003) Microstructure development during hot deformation of aluminium to large strains. Metall Mater Trans A 34:2737–2744
6. Kassner ME, Barrabes SR (2005) New developments in geometric dynamic recrystallization. Mater Sci Eng, A 410–411:152–155

7. De Pari L Jr, Misiolok WZ (2008) Theoretical predictions and experimental verification of surface grain structure evolution for AA6061 during hot rolling. *Acta Mater* 56:6174–6185
8. DEFORM-3D V6.1 User's manual, SFC, Columbus, Ohio, USA, 2007
9. Nes E (1998) Modelling of work hardening and stress saturation in fcc metals. *Prog Mater Sci* 41:129–193
10. Sherstnev P, Melzer C, Sommitsch C (2012) Prediction of precipitation kinetics during homogenisation and microstructure evolution during and after hot rolling of AA5083. *Int J Mech Sci* 54:12–19
11. Roters F, Raabe D, Gottstein G (2000) Work hardening in heterogeneous alloys—a microstructural approach based on three internal state variables. *Acta Mater* 48:4181–4189